

1           **The Positive Effect of Formaldehyde on the Photocatalytic**

2                           **Renoxification of Nitrate on TiO<sub>2</sub> Particles**

3  
4           Yuhan Liu, Xuejiao Wang, Mengshuang Sheng, Chunxiang Ye, Jing Shang\*

5           *State Key Joint Laboratory of Environmental Simulation and Pollution Control,*

6           *College of Environmental Sciences and Engineering, Peking University, 5 Yiheyuan*

7                           *Road, Beijing 100871, P. R. China*

8  
9           Corresponding author: Jing Shang

10          Email: shangjing@pku.edu.cn

11  
12          **Abstract**

13           Renoxification is the process of recycling of NO<sub>3</sub><sup>-</sup>/HNO<sub>3</sub> into NO<sub>x</sub> under  
14          illumination, which is mostly ascribed to the photolysis of nitrate. TiO<sub>2</sub>, a typical  
15          mineral dust component, can play its photocatalytic role in “renoxification” process  
16          due to NO<sub>3</sub> radical formed, and we define this process as “photocatalytic  
17          renoxification”. Formaldehyde (HCHO), the most abundant carbonyl compound in  
18          the atmosphere, may participate in the renoxification of nitrate-doped TiO<sub>2</sub> particles.  
19          In this study, we established an environmental chamber reaction system with the  
20          presence of HCHO and nitrate-doped TiO<sub>2</sub>. The direct photolyses of both nitrate and  
21          NO<sub>3</sub> radical were excluded by adjusting the illumination wavelength, so as to explore  
22          the effect of HCHO on the “photocatalytic renoxification”. It is found that NO<sub>x</sub>

23 concentration can reach up to more than 100 ppb for nitrate-doped TiO<sub>2</sub> particles,  
24 while almost no NO<sub>x</sub> was generated in the absence of HCHO. Nitrate type, relative  
25 humidity and HCHO concentration were found to influence NO<sub>x</sub> release. Adsorbed  
26 HCHO may react with nitrate radicals through hydrogen abstraction to form adsorbed  
27 HNO<sub>3</sub> on the surface, which is responsible for the release of NO<sub>x</sub>. The mass  
28 generation of NO<sub>x</sub> was suggested to via the NO<sub>3</sub><sup>-</sup>-NO<sub>3</sub><sup>·</sup>-HCHO-HNO<sub>3</sub>-NO<sub>x</sub> pathway,  
29 with HCHO and TiO<sub>2</sub> exhibiting a significant synergistic effect. Our proposed  
30 reaction mechanism by which HCHO promotes photocatalytic renoxification is  
31 helpful for deeply understanding the atmospheric photochemical processes and  
32 nitrogen cycling.

### 33 **1 Introduction**

34 The levels of ozone (O<sub>3</sub>) and hydroxyl radicals (·OH) in the troposphere can be  
35 promoted by nitrogen oxides (NO<sub>x</sub> = NO + NO<sub>2</sub>), such that NO<sub>x</sub> plays an important  
36 role in the formation of secondary aerosols and atmospheric oxidants (Platt et al.,  
37 1980; Stemmler et al., 2006; Harris et al., 1982; Finlayson-Pitts and Pitts, 1999). NO<sub>x</sub>  
38 can be converted into nitric acid (HNO<sub>3</sub>) and nitrate (NO<sub>3</sub><sup>-</sup>) through a series of  
39 oxidation and hydrolysis reactions and is eventually removed from the atmosphere  
40 through subsequent wet or dry deposition (Dentener and Crutzen, 1993; Goodman et  
41 al., 2001; Monge et al., 2010; Bedjanian and El Zein, 2012). However, comparisons  
42 of observations and modeling results for the marine boundary layer, land, and free  
43 troposphere (Read et al., 2008; Lee et al., 2009; Seltzer et al., 2015) have shown  
44 underestimation of HNO<sub>3</sub> or NO<sub>3</sub><sup>-</sup> content, NO<sub>x</sub> abundance, and NO<sub>x</sub>/HNO<sub>3</sub> ratios,

45 indicating the presence of a new, rapid  $\text{NO}_x$  circulation pathway (Ye et al., 2016b;  
46 Reed et al., 2017). Some researchers have suggested that deposited  $\text{NO}_3^-$  and  $\text{HNO}_3$   
47 can be recycled back to gas phase  $\text{NO}_x$  under illumination, via the renoxification  
48 process (Schuttlefield et al., 2008; Romer et al., 2018; Bao et al., 2020; Shi et al.,  
49 2021). Photolytic renoxification occurs under light with a wavelength of  $< 350$  nm,  
50 through the photolysis of  $\text{NO}_3^-/\text{HNO}_3$  adsorbed on the solid surface to generate  $\text{NO}_x$ .  
51 Notably, the photolysis of  $\text{NO}_3^-/\text{HNO}_3$  is reported to occur at least 2 orders of  
52 magnitude faster on different solid surfaces (natural or artificial) or aerosols than in  
53 the gas phase (Ye et al., 2016a; Zhou et al., 2003; Baergen and Donaldson, 2013).  
54 Several recent studies have shown that renoxification has important atmospheric  
55 significance (Deng et al., 2010; Kasibhatla et al., 2018; Romer et al., 2018; Alexander  
56 et al., 2020), providing the atmosphere with a new source of photochemically reactive  
57 nitrogen species, i.e., HONO or  $\text{NO}_x$ , resulting in the production of more  
58 photooxidants such as  $\text{O}_3$  or  $\cdot\text{OH}$  (Ye et al., 2017), which further oxidize volatile  
59 organic compounds (VOCs), leading to the formation of more chromophores, thereby  
60 affecting the photochemical process (Bao et al., 2020).

61         Renoxification processes have recently been observed on different types of  
62 atmospheric particles, such as urban grime and mineral dust (Ninneman et al., 2020;  
63 Bao et al., 2018; Baergen and Donaldson, 2013; Ndour et al., 2009). Atmospheric  
64 titanium dioxide ( $\text{TiO}_2$ ) is mainly derived from windblown mineral dust, with mass  
65 mixing ratios ranging from 0.1 to 10% (Chen et al., 2012).  $\text{TiO}_2$  is widely used in  
66 industrial processes and building exteriors for its favorable physical and chemical

67 properties. Titanium and nitrate ions have been found to coexist in atmospheric  
68 particulates in different regions worldwide (Sun et al., 2005; Schwartz-Narbonne et al.,  
69 2019). The relative content of  $\text{TiO}_2$  and  $\text{NO}_3^-$  in atmospheric particles varies greatly,  
70 and nitrate-coated  $\text{TiO}_2$  ( $\text{NO}_3^-$ - $\text{TiO}_2$ ) aerosols containing  $\text{TiO}_2$  as the main body can  
71 be used to effectively represent particles for sandstorm modeling (Sun et al., 2005;  
72 Kim et al., 2012).  $\text{TiO}_2$  is a semiconductor metal oxide that can facilitate the  
73 photolysis of nitrate and the release of  $\text{NO}_x$  due to its photocatalytic activity (Ndour et  
74 al., 2009; Chen et al., 2012; Verbruggen, 2015; Schwartz-Narbonne et al., 2019).  
75 Under ultraviolet (UV) light,  $\text{TiO}_2$  generates electron-hole pairs in the conduction and  
76 valence bands, respectively (Linsebigler et al., 1995). Nitrate ions adsorbed at the  
77 oxide surface react with the photogenerated holes ( $h^+$ ) to form nitrate radicals ( $\text{NO}_3^\cdot$ ),  
78 which are subsequently photolyzed to  $\text{NO}_x$ , mainly under visible light illumination  
79 (Schuttlefield et al., 2008; George et al., 2015; Schwartz-Narbonne et al., 2019). Thus,  
80 the renoxification of  $\text{NO}_3^-$  is faster on  $\text{TiO}_2$  than on other oxides in mineral dust  
81 aerosols such as  $\text{SiO}_2$  or  $\text{Al}_2\text{O}_3$  (Lesko et al., 2015; Ma et al., 2021). In this study, we  
82 refer to renoxification involving  $h^+$  and  $\text{NO}_3^-$  in the reaction as photocatalytic  
83 renoxification based on the photocatalytic properties of  $\text{TiO}_2$ .

84 Many previous studies have focused mainly on particulate nitrate- $\text{NO}_x$   
85 photochemical cycling reactions, despite the potential impact of other reactant gases  
86 in the atmosphere. Formaldehyde (HCHO), the most abundant carbonyl compound in  
87 the atmosphere, which can react at night with  $\text{NO}_3^\cdot$  via hydrogen abstraction reactions  
88 to form  $\text{HNO}_3$  (Atkinson, 1991). Our previous study showed that the degradation rate

89 of HCHO was faster on  $\text{NO}_3^-$ - $\text{TiO}_2$  aerosols than on  $\text{TiO}_2$  particles, perhaps as a result  
90 of HCHO oxidation by  $\text{NO}_3\cdot$  (Shang et al., 2017). To date, no studies have reported the  
91 effect of HCHO on photocatalytic renoxification. Adsorbed HCHO would react with  
92  $\text{NO}_3\cdot$  generated on the  $\text{NO}_3^-$ - $\text{TiO}_2$  aerosol surface, thus alter the surface nitrogenous  
93 species and renoxification process. The present study is the first to explore the  
94 combined effect of HCHO and photocatalytic  $\text{TiO}_2$  particles on the renoxification of  
95 nitrate. The wavelengths of the light sources were adjusted to exclude photolytic  
96 renoxification while making photocatalytic renoxification available for better  
97 elucidate the reaction mechanism. We investigated the effects of various influential  
98 factors including nitrate type, nitrate content, RH, and initial HCHO concentration, to  
99 understand the atmospheric renoxification of nitrate in greater detail.

## 100 **2 Methods**

### 101 **2.1 Environmental chamber setup**

102 Details of the experimental apparatus and protocol used in the current study have  
103 been previously described (Shang et al., 2017). Briefly, the main body of the  
104 environmental chamber is a 400 L polyvinyl fluoride (PVF) bag filled with synthetic  
105 air (high purity  $\text{N}_2$  (99.999%) mixed with high purity  $\text{O}_2$  (99.999%) in the ratio of  
106 79:21 by volume, Beijing Huatong Jingke Gas Chemical Co.). The chamber is  
107 capable of temperature ( $\sim 293$  K) and relative humidity (0.8–70%) control using a  
108 water bubbler and air conditioners, respectively. The chamber is equipped with two  
109 light sources both with the central wavelength of 365 nm. One is a set of 36 W tube  
110 lamps with a main spectrum of 320–400 nm and a small amount of 480–600 nm

111 visible light (Figure S1a). The other is a set of 12 W Light-emitting diode (LED)  
112 lamps with a narrow main spectrum of 350-390 nm (Figure S1b). The light intensities  
113 for the tube and LED lamp at 365 nm were  $300 \mu\text{W}\cdot\text{cm}^{-2}$  and  $200 \mu\text{W}\cdot\text{cm}^{-2}$ ,  
114 respectively, measured in the middle of the chamber.  $\text{NO}_x$  concentrations at the outlet  
115 of the chamber were monitored by a chemiluminescence  $\text{NO}_x$  analyzer (ECOTECH,  
116 EC9841B). HCHO was generated by thermolysis of paraformaldehyde at  $70^\circ\text{C}$  and  
117 detected via acetyl acetone spectrophotometric method using a UV-Vis  
118 spectrophotometer (PERSEE, T6) or a fluorescence spectrophotometer (THERMO,  
119 Lumina), depending on different initial HCHO concentrations. The particle size  
120 distribution was measured by a Scanning Nano Particle Spectrometer (HCT,  
121 SNPS-20). Electron Spin Resonance (Nuohai Life Science, MiniScope MS 5000) was  
122 used to measure  $\cdot\text{OH}$  on the surface of particles. 5,5-dimethyl-1-pyrroline-N-oxide  
123 (DPMO, Enzo) was used as the capture agent.  $50 \mu\text{L}$  particle-containing suspension  
124 mixed with  $50 \mu\text{L}$  DMPO (concentration of  $200 \mu\text{M}$ ) was loaded in a 1 mm capillary.  
125 Four 365 nm LED lamps were placed side by side vertically at a distance of about 1  
126 cm from the capillary, and the measurement was carried out after 1 min of irradiation.  
127 The modulation frequency was 100 kHz, the modulation amplitude was 0.2 mT, the  
128 microwave power was 10 mW and the sweep time was 60 s.

## 129 **2.2 Nitrate- $\text{TiO}_2$ composite samples**

130 In our experiments, two nitrate salts, potassium nitrate (AR, Beijing Chemical  
131 Works Co., Ltd) or ammonium nitrate (AR, Beijing Chemical Works Co., Ltd), were  
132 complexed with pure  $\text{TiO}_2$  ( $\geq 99.5\%$ , Degussa AG) powder or  $\text{TiO}_2$  (1 wt.%)/ $\text{SiO}_2$

133 mixed powder to prepare  $\text{NO}_3^-$ - $\text{TiO}_2$  or  $\text{NO}_3^-$ - $\text{TiO}_2$  (1 wt.%)/ $\text{SiO}_2$  samples. 250 mg  
134  $\text{TiO}_2$  was simply mixed in nitrate solutions at the desired mass mixing ratio (with  
135 nitrate content of 4 wt.%) to obtain a mash. The mash was dried at 90 °C and then  
136 ground carefully for 30 min. A series of samples with different amount of nitrate were  
137 prepared and diffuse reflectance fourier transform infrared spectroscopy (DRIFTS)  
138 measurements were made to test their homogeneity. Figure S2 shows DRIFTS spectra  
139 of these  $\text{KNO}_3$ - $\text{TiO}_2$  composites, of which  $1760\text{ cm}^{-1}$  peak is one of the typical  
140 vibrating peaks of nitrate (Aghazadeh, 2016; Maeda et al., 2011). Ratio value of peak  
141 area from  $1730$ - $1790\text{ cm}^{-1}$  for 1, 4, 32, 80 wt.% composited samples is 1: 4.1: 29.8:  
142 81.6, which is very close to that of theoretical value, proving that the samples were  
143 uniformly mixed.  $\text{SiO}_2$  (AR, Xilong Scientific Co., Ltd.) with no optical activity was  
144 also chosen for comparison, and samples of  $\text{KNO}_3$ - $\text{SiO}_2$  and  $\text{KNO}_3$ - $\text{TiO}_2$ (1  
145 wt.%)/ $\text{SiO}_2$  samples with a potassium nitrate content of 4 wt.% were prepared. The  
146 blank 250 mg  $\text{TiO}_2$  sample was solved in pure water with the same procedure as  
147 mentioned above. 4 wt.%  $\text{HNO}_3$ - $\text{TiO}_2$  composite particles were prepared for  
148 comparison. Concentrated nitric acid (AR, Beijing Chemical Works Co., Ltd) was  
149 diluted to 1 M and 250 mg  $\text{TiO}_2$  was added to the nitric acid solution and stirred  
150 evenly. A layer of aluminum foil was covered on the surface of the  $\text{HNO}_3$ - $\text{TiO}_2$   
151 homogenate and dried naturally in the room. After air-drying, follow the same steps  
152 above to grind for use. We also selected Arizona Test Dust (ATD, Powder Technology  
153 Inc.), whose chemical composition and weight percentage were shown in Table S1, as  
154 a substitute of  $\text{NO}_3^-$ / $\text{TiO}_2$  to investigate the “photocatalytic renoxification” process of

155 nitrate and the positive effect of HCHO.

### 156 **2.3 Environmental chamber experiments**

157 For the chamber operation, we completely evacuated the chamber after every  
158 experiment, then cleaned the chamber walls with deionized water and then dried by  
159 flushing the chamber with ultra-zero air to remove any particles or gases collected on  
160 the chamber walls. The experiments carried out in the environmental chamber can be  
161 divided into two categories according to whether HCHO was involved or not. (1) No  
162 HCHO involvement in the reaction. The PVF bag was inflated by 250L synthetic air,  
163 and then 75 mg particles were instantly sprayed into the chamber by a transient  
164 high-pressure airflow. As shown in Figure S3, the concentration of 4 wt.%  
165  $\text{KNO}_3\text{-TiO}_2$  particles decreased rapidly due to the sedimentation of the larger particles  
166 and the electrostatic adsorption of the particles by the environmental chamber. The  
167 size distribution reached stable after about 60 min with the peak particle size was  
168 about 120 nm, similar to that of atmospheric particles in some urban areas in China  
169 (Wang et al., 2015; Li et al., 2019). (2) With the participation of HCHO. The PVF bag  
170 was inflated by 125 L synthetic air, followed by the introduction of HCHO, and then  
171 the chamber was filled up with zero air to about 250 L. In order to know the HCHO  
172 adsorption before and after the particles' introduction, we conducted a conditional  
173 experiment in the dark. It can be seen from Figure S4 that it took about 90 min for the  
174 concentration of HCHO to reach stable, and can be sustained. Then, 75 mg  $\text{TiO}_2$  or  
175  $\text{NO}_3^-/\text{TiO}_2$  powders were introduced instantly and the concentration of HCHO  
176 decreased upon the introduction. It took about 60 min for HCHO to reach its second



177 adsorption equilibrium, and the concentration of HCHO can be stable for several  
178 hours in the dark. Therefore, for the irradiation experiments, the particles were  
179 injected at 90 min after HCHO's introduction, and the lamps were turned on at 60 min  
180 after the particle's introduction.

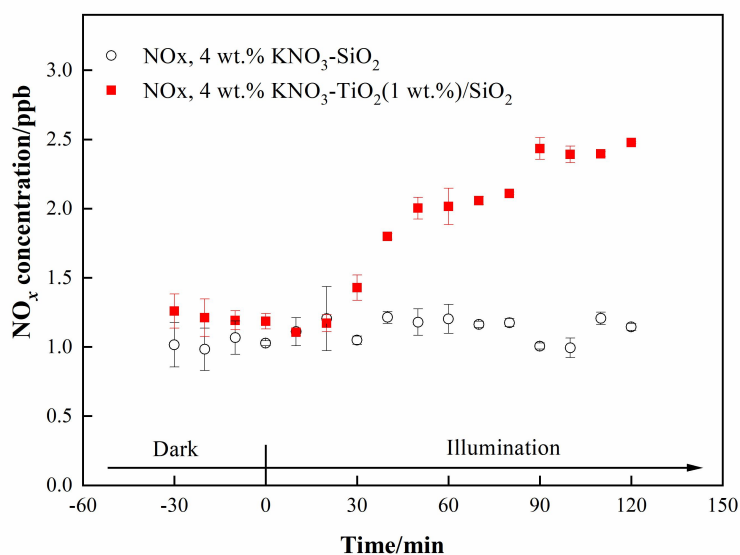
181 To determine the background value of  $\text{NO}_x$  in the reaction system, four blank  
182 experiments were carried out under illumination without nitrate: "synthetic air",  
183 "synthetic air +  $\text{TiO}_2$ ", "synthetic air + HCHO" and "synthetic air + HCHO +  $\text{TiO}_2$ ".  
184 In the blank experiments of "synthetic air" and "synthetic air +  $\text{TiO}_2$ ", the  $\text{NO}_x$   
185 concentration remained stable during 180 min illumination, and the concentration  
186 change was no more than 0.5 ppb (Figure S5a). Therefore, the environmental chamber,  
187 synthetic air and the surface of  $\text{TiO}_2$  particles were thought to be relatively clean, and  
188 there was no generation and accumulation of  $\text{NO}_x$  under illumination. When HCHO  
189 was introduced into the environmental chamber,  $\text{NO}_x$  accumulated ~2 ppb in 120 min  
190 with or without  $\text{TiO}_2$  particles (Figure S5b). Compared with the blank experiment  
191 results when there was no HCHO,  $\text{NO}_x$  might come from the generation process of  
192 HCHO (impurities in paraformaldehyde). However, considering the high  
193 concentration level of  $\text{NO}_x$  produced in the  $\text{NO}_3^-$ - $\text{TiO}_2$  system containing HCHO  
194 under the same conditions in this study (see later in Figure 2), the  $\text{NO}_x$  generated in  
195 this blank experiment can be negligible.

## 196 **3 Results and discussion**

### 197 **3.1 The positive effect of $\text{TiO}_2$ on the renoxification process**

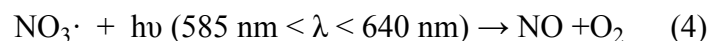
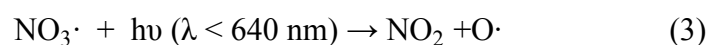
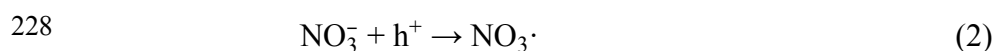
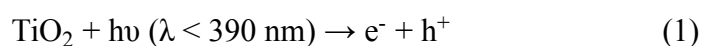
198 We investigated the photocatalytic role of  $\text{TiO}_2$  on renoxification. The light

199 source was two 365 nm tube lamps containing small amounts of 400–600 nm visible  
 200 light; this setup was suitable for exciting TiO<sub>2</sub> and the photolysis of available nitrate  
 201 radicals. Raw NO<sub>x</sub> data measured in the chamber under dark and illuminated  
 202 conditions for 4 wt.% KNO<sub>3</sub>-SiO<sub>2</sub> and 4 wt.% KNO<sub>3</sub>-TiO<sub>2</sub> (1 wt.%)/SiO<sub>2</sub> are shown  
 203 in Figure 1. The ratio of 1 wt. % TiO<sub>2</sub> to SiO<sub>2</sub> corresponds to their ratio in sand and  
 204 dust particles. We observed no NO<sub>x</sub> in the KNO<sub>3</sub>-SiO<sub>2</sub> sample under dark or  
 205 illumination, indicating very weak direct photolysis of nitrate under our 365 nm  
 206 tube-lamp illumination conditions. However, when the sample containing TiO<sub>2</sub>/SiO<sub>2</sub>  
 207 was illuminated, NO<sub>x</sub> continually accumulated in the chamber. This finding confirms  
 208 that NO<sub>x</sub> production arising from photodissociation of NO<sub>3</sub><sup>-</sup> on TiO<sub>2</sub>/SiO<sub>2</sub> was caused  
 209 by the photocatalytic property of TiO<sub>2</sub> (i.e., photocatalytic renoxification) and was not  
 210 due to the direct photolysis of NO<sub>3</sub><sup>-</sup> (photolytic renoxification).



211  
 212 **Figure 1.** Effect of illumination on the release of NO<sub>x</sub> from 4 wt.% KNO<sub>3</sub>-SiO<sub>2</sub> and 4  
 213 wt.% KNO<sub>3</sub>-TiO<sub>2</sub>(1 wt.%)/SiO<sub>2</sub> at 293 K and 0.8% of relative humidity. 365 nm tube  
 214 lamps were used during the illumination experiments.

215 TiO<sub>2</sub> can be excited by UV illumination to generate electron-hole pairs, and the  
216 h<sup>+</sup> can react with adsorbed NO<sub>3</sub><sup>-</sup> to produce NO<sub>3</sub><sup>·</sup> (Ndour et al., 2009). Thus, in the  
217 present study, NO<sub>3</sub><sup>·</sup> mainly absorbed visible light emitted from the tube lamps, which  
218 was subsequently photolyzed to NO<sub>x</sub> through Eqs. (3) and (4) (Wayne et al., 1991),  
219 which explains why NO<sub>x</sub> was observed in this study. Thus, we demonstrated that TiO<sub>2</sub>  
220 can be excited at illumination wavelengths of ~365 nm, even when the content was  
221 very low, and that NO<sub>x</sub> accumulated due to the production and further photolysis of  
222 NO<sub>3</sub><sup>·</sup>. However, the production rate of NO<sub>x</sub> was very slow, reaching only 1.3 ppb  
223 during 90 min of illumination. This result may have been caused by the blocking  
224 effect of K<sup>+</sup> on NO<sub>3</sub><sup>-</sup>. K<sup>+</sup> forms ion pairs with NO<sub>3</sub><sup>-</sup>, and electrostatic repulsion  
225 between K<sup>+</sup> and h<sup>+</sup> prevents NO<sub>3</sub><sup>-</sup> from combining with h<sup>+</sup> to generate NO<sub>3</sub><sup>·</sup> to a  
226 certain extent, thereby weakening the positive effect of TiO<sub>2</sub> on the renoxification of  
227 KNO<sub>3</sub> (Rosseler et al., 2013).



### 229 **3.2 The synergistic positive effect of TiO<sub>2</sub> and HCHO on the renoxification** 230 **process**

231 LED lamps with a wavelength range of 350–390 nm and no visible light were  
232 used to irradiate 4 wt.% KNO<sub>3</sub>-TiO<sub>2</sub> without generating NO<sub>x</sub> (NO<sub>2</sub> and NO  
233 concentrations fluctuate within the error range of the instrument) (Figure S6). TiO<sub>2</sub>

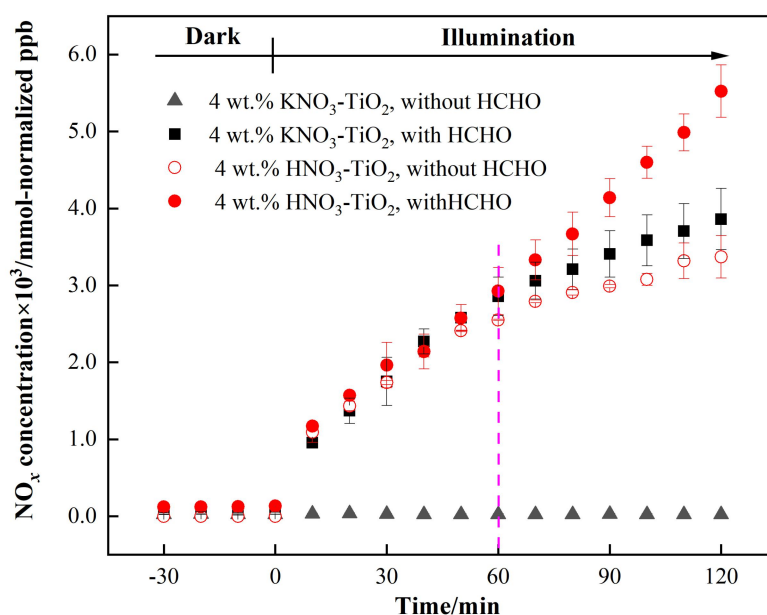
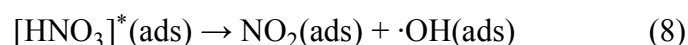
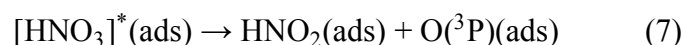
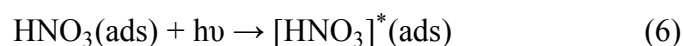
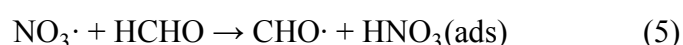
234 can be excited under this range of irradiation, producing  $\text{NO}_3$  radicals as discussed  
235 above. The lack of  $\text{NO}_x$  generation indicates that neither nitrate photolysis nor  
236  $\text{NO}_3\cdot$  photolysis occurred under 365 nm LED lamp illumination conditions. In  
237 addition, it has been shown that  $\text{NO}_3\cdot$  photolysis only occurs in visible light (Aldener  
238 et al., 2006). Therefore, the LED lamp setup was used in subsequent experiments to  
239 exclude the direct photolysis of both  $\text{KNO}_3$  and  $\text{NO}_3\cdot$ , but allow the excitation of  $\text{TiO}_2$ .  
240 This approach allowed us to investigate the process of photocatalytic renoxification  
241 caused by HCHO in the presence of photogenerated  $\text{NO}_3\cdot$ .

242 Atmospheric trace gases can undergo photocatalytic reactions on the surface of  
243  $\text{TiO}_2$  (Chen et al., 2012). As the illumination time increased, the concentration of  
244 HCHO showed a linear downward trend, which was found to fit zero-order reaction  
245 kinetics (Figure S7). The zero-order reaction rate constants of HCHO on  $\text{TiO}_2$  and 4  
246 wt.%  $\text{KNO}_3$ - $\text{TiO}_2$  particles were  $9.1 \times 10^{-3}$  and  $1.4 \times 10^{-2}$  ppm  $\text{min}^{-1}$ , respectively,  
247 which were much higher than that for gaseous HCHO photolysis (Shang et al., 2017).  
248 We suggested that the produced  $\text{NO}_3\cdot$  contributed to the enhanced uptake of HCHO.  
249 In the following study, the effect of HCHO on the photocatalytic renoxification of  
250  $\text{NO}_3^-$ - $\text{TiO}_2$  was explored.

251 Variation in  $\text{NO}_x$  concentration within the chamber containing nitrate- $\text{TiO}_2$   
252 particles with or without HCHO is shown in Figure 2. For 4 wt.%  $\text{KNO}_3$ - $\text{TiO}_2$   
253 particles, the  $\text{NO}_x$  concentration began to increase upon irradiation in the presence of  
254 HCHO, reaching  $\sim 3861$  mmol-normalized ppb (equivalent to 110 ppb) within 120  
255 min. This result indicates that HCHO greatly promoted photocatalytic renoxification

256 of  $\text{KNO}_3$  on the surfaces of  $\text{TiO}_2$  particles. This reaction process can be divided into  
257 two stages: a rapid increase within the first 60 min and a slower increase within the  
258 following 60 min, each consistent with zero-order reaction kinetics. The slow stage is  
259 due to the photodegradation of HCHO on  $\text{KNO}_3$ - $\text{TiO}_2$  aerosols, which led to a  
260 decrease in its concentration, gradually weakening the positive effect.  $\text{NO}_x$  is the sum  
261 of  $\text{NO}_2$  and  $\text{NO}$ , both of which showed a two-stage concentration increase (Figure S8).  
262 The  $\text{NO}_2$  generation rate was nearly 6 times that of  $\text{NO}$ , as compared to using the  
263 zero-order rate constant within 60 min ( $1.18 \text{ ppb min}^{-1} \text{ NO}_2$ ,  $R^2 = 0.96$ ;  $0.19 \text{ ppb}$   
264  $\text{min}^{-1} \text{ NO}$ ,  $R^2 = 0.91$ ). This burst-like generation of  $\text{NO}_x$  can be ascribed to the  
265 reaction between generated  $\text{NO}_3\cdot$  and HCHO via hydrogen abstraction to form  
266 adsorbed nitric acid ( $\text{HNO}_3(\text{ads})$ ) on  $\text{TiO}_2$  particles. We measured the pH of water  
267 extracts in  $\text{NO}_3^-$ - $\text{TiO}_2$  systems with and without HCHO. It was found that the pH  
268 decreased by 1.7% for  $\text{KNO}_3$ - $\text{TiO}_2$ , suggesting the formation of acidic species such as  
269  $\text{HNO}_3(\text{ads})$  in this study. Based on the analysis of the absorption cross section of  
270  $\text{HNO}_3$  adsorbed on fused silica surface, the  $\text{HNO}_3(\text{ads})$  absorption spectrum has been  
271 reported to be red-shifted compared to  $\text{HNO}_3(\text{g})$ , extending from 350 to 365 nm, with  
272 a simultaneous cross-sectional increase (Du and Zhu, 2011). Therefore,  $\text{HNO}_3(\text{ads})$   
273 was subjected to photolysis to produce  $\text{NO}_2$  and HONO (Eqs. (6)-(8)) under the LED  
274 lamp used in this study. A previous study of  $\text{HNO}_3$  photolysis on the surface of Pyrex  
275 glass showed that the ratio of the formation rates of photolysis products  
276 ( $J_{\text{NO}_x}/J_{(\text{NO}_x+\text{HONO})}$ ) was  $> 97\%$  at  $\text{RH} = 0\%$  (Zhou et al., 2003), suggesting that  $\text{NO}_x$  is  
277 the main gaseous product under dry conditions. Thus, the effect of HONO on product

278 distribution and  $\text{NO}_x$  concentration was negligible in this study. Together, these results  
 279 suggest that  $\text{NO}_3\cdot$  and  $\text{HCHO}$  generate  $\text{HNO}_3(\text{ads})$  on particle surfaces through  
 280 hydrogen abstraction, which contributes to the substantial release of  $\text{NO}_x$  via  
 281 photolysis. This photocatalytic renoxification via the  $\text{NO}_3^-$ - $\text{NO}_3\cdot$ - $\text{HCHO}$ - $\text{HNO}_3$ - $\text{NO}_x$   
 282 pathway is important considering the high abundance of hydrogen donor organics in  
 283 the atmosphere.



284

285 **Figure 2.** Effect of formaldehyde on the renoxification processes of different nitrate-  
 286 doped particles at 293 K and 0.8% of relative humidity. 365 nm LED lamps were used  
 287 during the illumination experiment. The initial concentration of  $\text{HCHO}$  was about 9  
 288 ppm.

289 To demonstrate the proposed HCHO mechanism and the photolysis contribution  
290 of HNO<sub>3</sub> to NO<sub>x</sub>, we prepared an HNO<sub>3</sub>-TiO<sub>2</sub> sample by directly dissolving TiO<sub>2</sub> into  
291 dilute nitric acid. The formation of NO<sub>x</sub> on HNO<sub>3</sub>-TiO<sub>2</sub> without HCHO under  
292 illumination was obvious and at a rate comparable with that on KNO<sub>3</sub>-TiO<sub>2</sub> with  
293 HCHO (Figure 2). The renoxification of HNO<sub>3</sub>-TiO<sub>2</sub> particles was further enhanced  
294 following the introduction of HCHO. This is because that HNO<sub>3</sub> dissociates on  
295 particle surfaces to generate NO<sub>3</sub><sup>-</sup>, such that HNO<sub>3</sub> exists on TiO<sub>2</sub> as both HNO<sub>3</sub>(ads)  
296 and NO<sub>3</sub><sup>-</sup>(ads). Similarly, NO<sub>3</sub><sup>-</sup>(ads) completed the NO<sub>3</sub><sup>-</sup>-NO<sub>3</sub><sup>·</sup>-HCHO-HNO<sub>3</sub>-NO<sub>x</sub>  
297 pathway as described above through the reaction process shown in Eqs. (2) to (8). The  
298 rates of NO<sub>x</sub> production from HNO<sub>3</sub>-TiO<sub>2</sub> particles with and without HCHO were  
299 similar for the first 60 min (Figure 2), mainly due to the direct photolysis of partial  
300 HNO<sub>3</sub>(ads). However, after 60 min, NO<sub>x</sub> was generated rapidly in the presence of  
301 HCHO, perhaps due to the dominant photocatalytic renoxification of NO<sub>3</sub><sup>-</sup>(ads).  
302 These findings indicate that HCHO converts NO<sub>3</sub><sup>-</sup> on particle surfaces into HNO<sub>3</sub>(ads)  
303 by reacting with NO<sub>3</sub><sup>·</sup>, and then HNO<sub>3</sub>(ads) photolyzes at a faster rate to generate  
304 NO<sub>x</sub>, allowing HCHO to enhance the formation of NO<sub>x</sub>. Overall, the photocatalytic  
305 renoxification of NO<sub>3</sub><sup>-</sup>-TiO<sub>2</sub> particles affects atmospheric oxidation and the nitrogen  
306 cycle, and the presence of HCHO further enhances this impact.

307 Photocatalytic renoxification reaction occurs on the surfaces of mineral dust due  
308 to the presence of semiconductor oxides with photocatalytic activity such as TiO<sub>2</sub>  
309 (Ndour et al., 2009). In order to confirm this, we synthesized nitrate with inert SiO<sub>2</sub> as  
310 a comparison. It can be seen from Figure S9 that no NO<sub>2</sub> formation was observed

311 whether HCHO was present or not, indicating that photocatalytically active particle  
312 TiO<sub>2</sub> is critical to the photocatalytic renoxification process. Furthermore, a kind of  
313 commercial mineral dust ATD was selected to study the effects of HCHO on this  
314 process. We detected ·OH in irradiated pure TiO<sub>2</sub> and ATD samples using electron  
315 spin resonance (ESR) technique, and found that for ATD samples, the peak intensity  
316 of ·OH generation was 40% that of TiO<sub>2</sub> samples (Figure S10). ·OH originates in the  
317 reaction of h<sup>+</sup> with surface adsorbed water (Ahmed et al., 2014). ATD contains  
318 semiconductor oxides such as TiO<sub>2</sub> and Fe<sub>2</sub>O<sub>3</sub>, and is thought to exhibit photocatalytic  
319 properties affecting the renoxification of nitrate. The NO<sub>3</sub><sup>-</sup> content of ATD is 4 × 10<sup>17</sup>  
320 molecules m<sup>-2</sup>, which is ~0.25 wt.% of the total mass (Huang et al., 2015; Jiyeon et  
321 al., 2017). The NO<sub>x</sub> concentration changes observed in the environmental chamber  
322 demonstrated that HCHO promoted the renoxification of ATD particles (Figure S11).  
323 This result suggests that mineral dust containing photocatalytic semiconductor oxides  
324 such as TiO<sub>2</sub>, Fe<sub>2</sub>O<sub>3</sub>, and ZnO can greatly promote the conversion of granular nitrate  
325 to NO<sub>x</sub> in the presence of HCHO.

326

### 327 **3.3 Influential factors on the photocatalytic renoxification process**

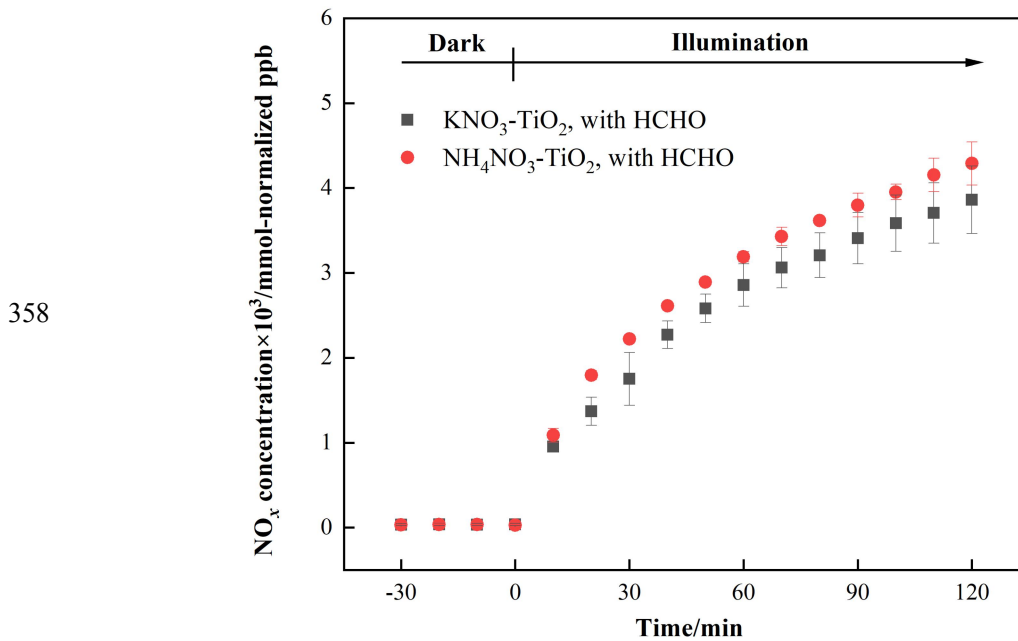
#### 328 **3.3.1 The influence of nitrate type**

329 As discussed above, HNO<sub>3</sub> and KNO<sub>3</sub> undergo different renoxification processes  
330 on the surface of TiO<sub>2</sub> under the same illumination conditions, suggesting that cations  
331 bound to NO<sub>3</sub><sup>-</sup> significantly affect NO<sub>x</sub> production. Different types of cations coexist  
332 with nitrate ions in atmospheric particulate matter, among which ammonium ions



333 (NH<sub>4</sub><sup>+</sup>) are important water-soluble ions that can be higher in content than K<sup>+</sup> in urban  
334 fine particulate matter (Zhou et al., 2016; Tang et al., 2021; Wang et al., 2021),  
335 especially in heavily polluted cities (Tian et al., 2020). Equal amounts of 4 wt.%  
336 NH<sub>4</sub>NO<sub>3</sub>-TiO<sub>2</sub> particles were introduced into the chamber and illuminated under the  
337 same conditions. Similar as Figure 2, millimole normalized ppb was used in order to  
338 compare the amount of NO<sub>x</sub> release for different kinds of nitrate with same percentage  
339 weight. It can be seen that HCHO had a much stronger positive effect on the release  
340 of NO<sub>x</sub> over NH<sub>4</sub>NO<sub>3</sub>-TiO<sub>2</sub> particles (Figure 3), which may be ascribed to NH<sub>4</sub><sup>+</sup>.  
341 Combined with the results of NH<sub>4</sub>NO<sub>3</sub>-TiO<sub>2</sub> and KNO<sub>3</sub>-TiO<sub>2</sub> particles, it seems that  
342 the affinity rather than electrostatic repulsion should be the primary effect of cations  
343 on the production of NO<sub>x</sub>. On substrates without photocatalytic activity such as SiO<sub>2</sub>  
344 and Al<sub>2</sub>O<sub>3</sub>, NH<sub>4</sub>NO<sub>3</sub> cannot generate NO<sub>x</sub>, (Ma et al., 2021) such that NO<sub>x</sub> production  
345 depends on the effect of TiO<sub>2</sub>. The h<sup>+</sup> generated by TiO<sub>2</sub> excitation reacts with  
346 adsorbed H<sub>2</sub>O to produce ·OH (Eq. (9)), which gradually oxidizes NH<sub>4</sub><sup>+</sup> to NO<sub>3</sub><sup>-</sup> (Eq.  
347 (10)). In our previous study, we demonstrated that irradiated (NH<sub>4</sub>)<sub>2</sub>SO<sub>4</sub>-TiO<sub>2</sub> samples  
348 had lower NH<sub>4</sub><sup>+</sup> and NO<sub>3</sub><sup>-</sup> peaks (Shang et al., 2017). Therefore, more NO<sub>3</sub><sup>-</sup>  
349 participated in the photocatalytic renoxification process via the  
350 NO<sub>3</sub><sup>-</sup>-NO<sub>3</sub>·-HCHO-HNO<sub>3</sub>-NO<sub>x</sub> pathway to generate NO<sub>x</sub>. Moreover, the results  
351 without HCHO are shown in Figure S12, both NH<sub>4</sub>NO<sub>3</sub>-TiO<sub>2</sub> particles and  
352 KNO<sub>3</sub>-TiO<sub>2</sub> particles produced almost no NO<sub>x</sub>, indicating the importance of HCHO  
353 for renoxification to occur. Due to the high content of NH<sub>4</sub>NO<sub>3</sub> in atmospheric  
354 particulate matter, the positive effect of HCHO on the photocatalytic renoxification

355 process may have some impact on the concentrations of NO<sub>x</sub> and other atmospheric  
 356 oxidants.



359 **Figure 3.** Effect of formaldehyde on the renoxification processes of 4 wt.%  
 360 NH<sub>4</sub>NO<sub>3</sub>-TiO<sub>2</sub> and 4 wt.% KNO<sub>3</sub>-TiO<sub>2</sub> particles at 293 K and 0.8% of relative  
 361 humidity. 365 nm LED lamps were used during the irradiation experiment. The initial  
 362 concentration of HCHO was about 9 ppm.

363

### 364 3.3.2 The influence of relative humidity

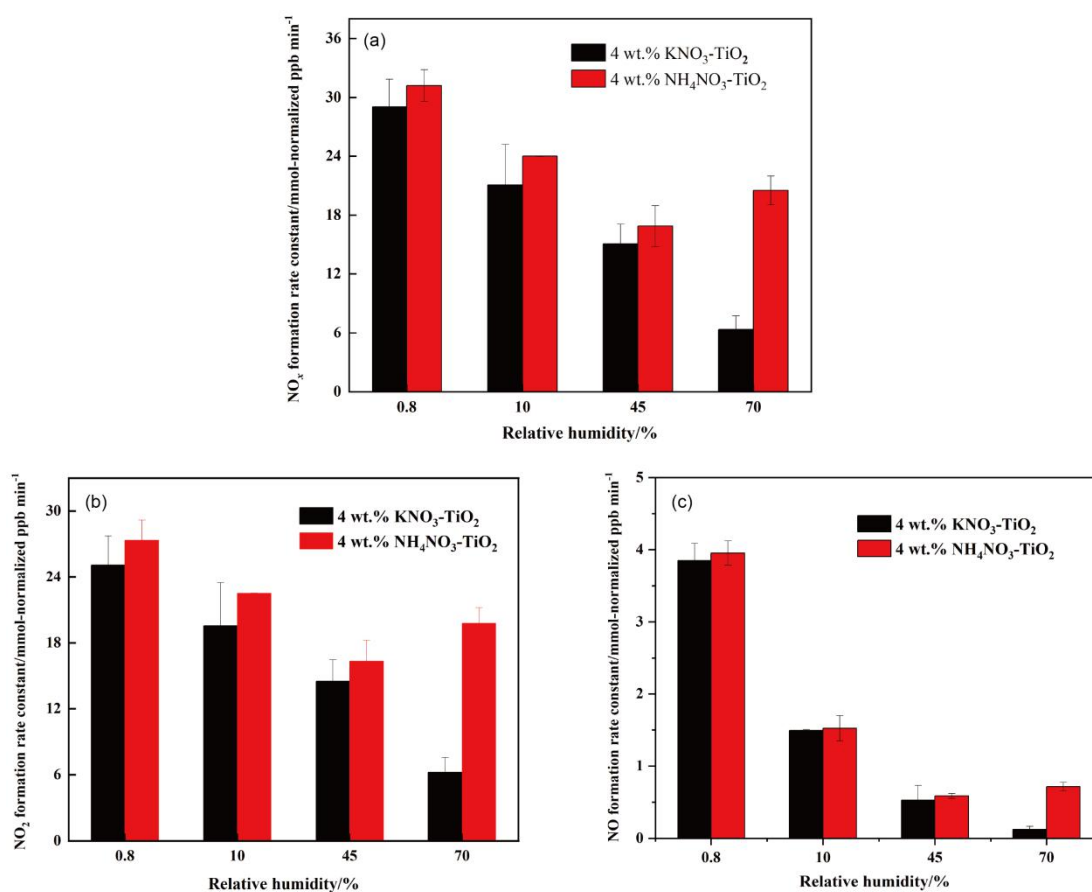
365 Water on particle surfaces can participate directly in the heterogeneous reaction  
 366 process. As shown in Eq. (9), H<sub>2</sub>O can be captured by h<sup>+</sup> to generate ·OH with strong  
 367 oxidizability in photocatalytic reactions. The first-order photolysis rate constant of  
 368 NO<sub>3</sub><sup>-</sup> on TiO<sub>2</sub> particles decreases by an order of magnitude, from  $(5.7 \pm 0.1) \times 10^{-4} \text{ s}^{-1}$

369 on dry surfaces to  $(7.1 \pm 0.8) \times 10^{-5} \text{ s}^{-1}$  when nitrate is coadsorbed with water above  
370 monolayer coverage (Ostaszewski et al., 2018). We explored the positive effect of  
371 HCHO on the  $\text{NO}_3^-$ - $\text{TiO}_2$  particle photocatalytic renoxification at different RH levels;  
372 the results are shown in Figure 4a. For  $\text{KNO}_3$ - $\text{TiO}_2$  particles, the rate of  $\text{NO}_x$   
373 production decreased as the RH of the environmental chamber increased, indicating  
374 that increased water content in the gas phase hindered photocatalytic renoxification  
375 for two reasons:  $\text{H}_2\text{O}$  competes with  $\text{NO}_3^-$  for  $\text{h}^+$  on the surface of  $\text{TiO}_2$  to  
376 generate  $\cdot\text{OH}$ , reducing the generation of  $\text{NO}_3\cdot$ , and competitive adsorption between  
377  $\text{H}_2\text{O}$  and HCHO causes the generated  $\cdot\text{OH}$  to compete with  $\text{NO}_3\cdot$  for HCHO,  
378 hindering the formation of  $\text{HNO}_3(\text{ads})$  on particle surfaces. Moreover, it is also  
379 possible that the loss of  $\text{NO}_x$  on the wall increases under high humidity conditions,  
380 resulting in a decrease in its concentration. This competitive process also occurs on  
381 the surface of  $\text{NH}_4\text{NO}_3$ - $\text{TiO}_2$  particles, but at  $\text{RH} = 70\%$ , the  $\text{NO}_x$  generation rate  
382 constant is slightly higher. The deliquescent humidity of  $\text{NH}_4\text{NO}_3$  at 298 K is  $\sim 62\%$ ,  
383 such that  $\text{NH}_4\text{NO}_3$  had already deliquesced at  $\text{RH} = 70\%$ , forming an  $\text{NH}_4^+/\text{NH}_3$ - $\text{NO}_3^-$   
384 liquid system on the particle surfaces. This quasi-liquid phase improved the dispersion  
385 of  $\text{TiO}_2$  in  $\text{NH}_4\text{NO}_3$ , resulting in greater  $\text{NO}_x$  release. The deliquescent humidity of  
386  $\text{KNO}_3$ - $\text{TiO}_2$  was  $> 90\%$ ,(2009) such that no phase change occurred at  $\text{RH} = 70\%$ , and  
387 the renoxification reaction rate retained a downward trend. In the presence of  $\text{H}_2\text{O}$ , in  
388 addition to the  $\text{NO}_3^-$ - $\text{NO}_3\cdot$ -HCHO- $\text{HNO}_3$  pathway observed in this study, there are a  
389 variety of  $\text{HNO}_3$  generation paths, such as the hydrolysis of  $\text{N}_2\text{O}_5$  via the  
390  $\text{NO}_2$ - $\text{N}_2\text{O}_5$ - $\text{HNO}_3$  pathway (Brown et al., 2005), the oxidation of  $\text{NO}_2$  by  $\cdot\text{OH}$

391 (Burkholder et al., 1993), and the reaction of  $\text{NO}_3\cdot$  with  $\text{H}_2\text{O}$  (Schutze and Herrmann,  
392 2005), all of which require further consideration and study.

393 The formation rates of NO and  $\text{NO}_2$  are shown in Figure 4b and c, respectively.  
394  $\text{NO}_2$  was the main product of surface  $\text{HNO}_3$  photolysis. Under humid conditions,  
395 generated  $\text{NO}_2(\text{ads})$  continued to react with  $\text{H}_2\text{O}$  adsorbed on the surface to form  
396  $\text{HONO}(\text{ads})$ . HONO was desorbed from the surface and released into the gas phase  
397 (Zhou et al., 2003; Bao et al., 2018; Pandit et al., 2021), providing gaseous HONO to  
398 the reaction system. Because the  $\text{NO}_x$  concentration remained high, the effect of  
399 HONO on  $\text{NO}_x$  analyzer results was negligible (Shi et al., 2021). As  $\text{NO}_2$  can form  
400  $\text{NO}_2^-$  with  $e^-$ , a reverse reaction also occurred between  $\text{NO}_2^-$  and HONO in the  
401 presence of  $\text{H}_2\text{O}$  (Ma et al., 2021; Garcia et al., 2021). Therefore, the increase in  $\text{H}_2\text{O}$   
402 increased the proportion of HONO in the nitrogen-containing products, such that the  
403  $\text{NO}_x$  generation rate decreased as RH increased. Comparing Figure 4b and c shows  
404 that, as RH increased, the NO production rate constant decreased more than that of  
405  $\text{NO}_2$ . HONO and  $\text{NO}_2$  generated by the photolysis of  $\text{HNO}_3(\text{ads})$  decreased  
406 accordingly, i.e., the NO source decreased. However, generated  $\text{NO}_2$  and NO  
407 underwent photocatalytic oxidation on the surface of  $\text{TiO}_2$ , and NO photodegradation  
408 was more significant under the same conditions (Hot et al., 2017). Generally, a certain  
409 amount of HONO will be generated during the reaction between HCHO and  
410  $\text{NO}_3^-$ - $\text{TiO}_2$  particles when RH is high, which affects the concentrations of  
411 atmospheric  $\cdot\text{OH}$ ,  $\text{NO}_x$ , and  $\text{O}_3$ . This process is more likely to occur in summer due to  
412 high RH and light intensity affecting atmospheric oxidation. In drier winters or dusty

413 weather, when TiO<sub>2</sub> content is high, HCHO greatly promotes the photocatalytic  
 414 renoxification of NO<sub>3</sub><sup>-</sup>-TiO<sub>2</sub> particles, thereby releasing more NO<sub>x</sub> into the atmosphere,  
 415 affecting the global atmospheric nitrogen budget. Thus, regardless of the seasonal and  
 416 regional changes, renoxification has significant practical importance.



417  
 418 **Figure 4.** Effect of relative humidity on the release of NO<sub>x</sub> (a), NO<sub>2</sub> (b), NO (c) over 4  
 419 wt.% NH<sub>4</sub>NO<sub>3</sub>-TiO<sub>2</sub> and 4 wt.% KNO<sub>3</sub>-TiO<sub>2</sub> particles at 293 K. 365 nm LED lamps  
 420 were used during the illumination experiment. The initial concentration of HCHO was  
 421 about 9 ppm.

### 422 3.3.3 The influence of initial HCHO concentration

423 To explore whether HCHO promotes nitrate renoxification at natural  
 424 concentration levels, we reduced the initial concentration of HCHO in the

425 environmental chamber by a factor of 10, to ~1.0 ppm. The positive effect of HCHO  
426 on the photocatalytic renoxification of  $\text{KNO}_3\text{-TiO}_2$  particles was clearly weakened,  
427 with  $\text{NO}_2$  concentration first increasing and then decreasing, and  $\text{NO}$  concentration  
428 remaining stable (Figure S13). The HCHO concentration decreased due to its  
429 consumption during the reaction, making its positive effect decline quickly. The  
430 photocatalytic oxidation reaction between  $\text{NO}_x$  and photogenerated reactive oxygen  
431 species (ROS) on the  $\text{TiO}_2$  surface further decreased the  $\text{NO}_x$  concentration.  
432 Photocatalytic oxidation of  $\text{NO}_x$  by ROS on  $\text{TiO}_2$  particles occurred at an HCHO  
433 concentration of 9 ppm, but the positive effect of HCHO remained dominant. Thus,  
434 no decrease in  $\text{NO}_x$  concentration was observed within 120 min in our experiments.

435 The concentration of HCHO in the atmosphere is relatively low, with a balance  
436 between the photocatalytic oxidation decay of  $\text{NO}_x$  and the release of  $\text{NO}_x$  via  
437 photocatalytic renoxification. The mutual transformation between particulate  $\text{NO}_3^-$   
438 and gaseous  $\text{NO}_x$  is more complex. The effect of low-concentration HCHO on the  
439 renoxification of  $\text{NO}_3^-$ - $\text{TiO}_2$  particles requires further investigation. However, many  
440 types of organics provide hydrogen atoms in the atmosphere, including alkanes (e.g.,  
441 methane and n-hexane), aldehydes (e.g., acetaldehyde), alcohols (e.g., methanol and  
442 ethanol), and aromatic compounds (e.g., phenol) that react with  $\text{NO}_3^-$  to produce nitric  
443 acid (Atkinson, 1991). These organics, together with HCHO, play similar positive  
444 roles in photocatalytic renoxification and, therefore, influence  $\text{NO}_x$  concentrations.

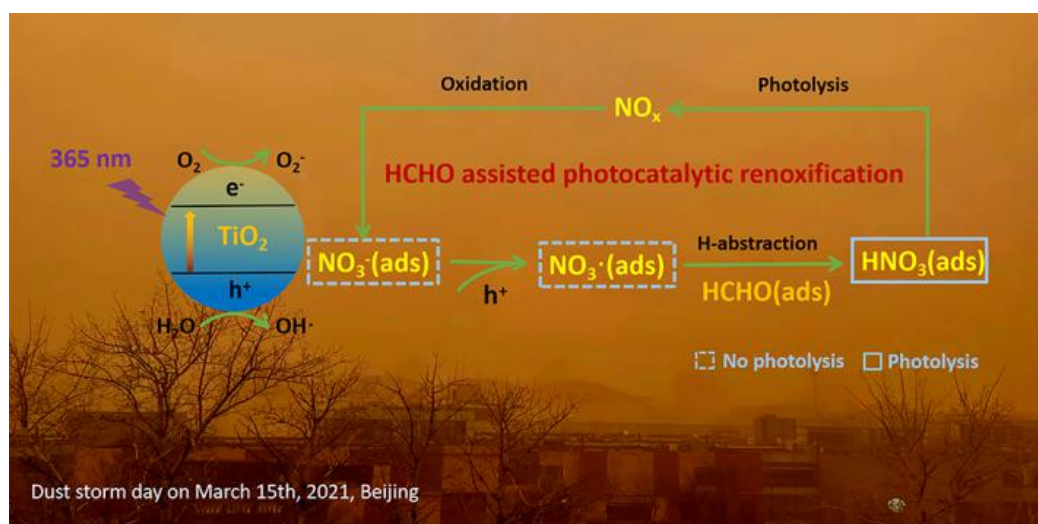
445

446

#### 447 **4 Atmospheric implications**

448 Nitric acid and nitrate are not only the final sink of  $\text{NO}_x$  in the atmosphere but  
449 are also among its important sources.  $\text{NO}_x$  from nitrate through renoxification is easily  
450 overlooked. The renoxification of nitrate on the surface of  $\text{TiO}_2$  particles can be  
451 divided into photolytic renoxification and photocatalytic renoxification. The  
452 photocatalytic performance of  $\text{TiO}_2$  promotes the renoxification process, which  
453 explains the influence of semiconducting metal oxide components on atmospheric  
454 mineral particles during the renoxification of nitrate. Although most previous studies  
455 have focused on solid-phase nitrate renoxification, our exploration of the roles of  
456 HCHO in this study will allow us to examine complex real-world pollution scenarios,  
457 in which multiple atmospheric pollutants coexist, as well as the effects of organic  
458 pollutants on the renoxification process. Atmospheric HCHO is taken up at the  
459 surface of particulate matter, accounting for up to ~50% of its absorption (Li et al.,  
460 2014), such that the heterogeneous participation of HCHO during renoxification is  
461 important. This study is the first to report that HCHO has a positive effect on the  
462 photocatalytic renoxification of nitrate on  $\text{TiO}_2$  particles, via the  
463  $\text{NO}_3^-$ - $\text{NO}_3^\cdot$ -HCHO- $\text{HNO}_3$ - $\text{NO}_x$  pathway (Figure 5), further increasing the release of  
464  $\text{NO}_x$  and other nitrogen-containing active species, which in turn affects the  
465 photochemical cycle of reactive radicals in the atmosphere and the formation of  
466 important atmospheric oxidants such as  $\text{O}_3$ . Although in the case of high  
467 concentrations of HCHO in our experiment, the response to the real situation will be  
468 biased, the results of this study illustrate a possible way of HCHO in influencing

469 nitrate renoxification in the atmosphere. Factors such as particulate matter  
 470 composition, RH, and initial HCHO concentration all influence the positive effect of  
 471 HCHO; notably, H<sub>2</sub>O competes with NO<sub>3</sub><sup>-</sup> for photogenerated holes. Based on these  
 472 findings, two balance systems should be explored in depth: the influence of RH on the  
 473 generation rates of HONO and NO<sub>x</sub>, as water increases the proportion of HONO in  
 474 nitrogen-containing products; and the balance between the photocatalytic degradation  
 475 of generated NO<sub>x</sub> on TiO<sub>2</sub> particles and the positive effect of HCHO on NO<sub>x</sub>  
 476 generation at low HCHO concentrations.



477  
 478 **Figure 5.** Positive role of HCHO on the photocatalytic renoxification of nitrate-TiO<sub>2</sub>  
 479 composite particles via the NO<sub>3</sub><sup>-</sup>-NO<sub>3</sub>·-HCHO-HNO<sub>3</sub>-NO<sub>x</sub> pathway.

480 Based on our results, we conclude that in photochemical processes on the  
 481 surfaces of particles containing semiconductor oxides, with the participation of  
 482 hydrogen donor organics, a significant synergistic photocatalytic renoxification  
 483 enhancement effect alters the composition of surface nitrogenous species via the  
 484 NO<sub>3</sub><sup>-</sup>-NO<sub>3</sub>·-hydrogen donor-HNO<sub>3</sub>-NO<sub>x</sub> pathway, thereby affecting atmospheric  
 485 oxidation and nitrogen cycling. The positive effect of HCHO can be extended from



486 TiO<sub>2</sub> in this study to other components of mineral dust such as Fe<sub>2</sub>O<sub>3</sub> and ZnO with  
487 photocatalytic activity, which may have practical applications. Our proposed reaction  
488 mechanism by which HCHO promotes photocatalytic renoxification will improve  
489 existing atmospheric chemistry models and reduce discrepancies between model  
490 simulations and field observations.

491

#### 492 ***Supplement.***

493 Detailed information of Figures S1-13 (which include the spectra of the lamps,  
494 DRIFTS spectra of KNO<sub>3</sub>-TiO<sub>2</sub> particles, size distribution of KNO<sub>3</sub>-TiO<sub>2</sub> particles,  
495 changes of HCHO concentration in the chamber, changes of NO<sub>x</sub> concentration under  
496 different reaction conditions, photodegradation curves of HCHO, ESR spectra of TiO<sub>2</sub>  
497 and ATD particles), and Table S1 (which demonstrates ATD chemical composition) .

498

#### 499 ***Acknowledgments***

500 The authors are grateful to the financial support provided by National Natural  
501 Science Foundation of China (Nos 41961134034, 21876003 and 21277004), and the  
502 Second Tibetan Plateau Scientific Expedition and Research (No. 2019QZKK0607).

503

#### 504 **References**

505 Aghazadeh, M.: Preparation of Gd<sub>2</sub>O<sub>3</sub> Ultrafine Nanoparticles by Pulse  
506 Electrodeposition Followed by Heat-treatment Method, Journal of Ultrafine Grained  
507 and Nanostructured Materials, 49, 80-86, 10.7508/jufgnsm.2016.02.04, 2016.

508 Ahmed, A. Y., Kandiel, T. A., Ivanova, I., and Bahnemann, D.: Photocatalytic and

509 photoelectrochemical oxidation mechanisms of methanol on TiO<sub>2</sub> in aqueous solution,  
510 Applied Surface Science, 319, 44-49, 10.1016/j.apsusc.2014.07.134, 2014.

511 Aldener, M., Brown, S. S., Stark, H., Williams, E. J., Lerner, B. M., Kuster, W. C.,  
512 Goldan, P. D., Quinn, P. K., Bates, T. S., Fehsenfeld, F. C., and Ravishankara, A. R.:  
513 Reactivity and loss mechanisms of NO<sub>3</sub> and N<sub>2</sub>O<sub>5</sub> in a polluted marine environment:  
514 Results from in situ measurements during New England Air Quality Study 2002,  
515 Journal of Geophysical Research-Atmospheres, 111, D23S73, 10.1029/2006jd007252,  
516 2006.

517 Alexander, B., Sherwen, T., Holmes, C. D., Fisher, J. A., Chen, Q., Evans, M. J., and  
518 Kasibhatla, P.: Global inorganic nitrate production mechanisms: comparison of a  
519 global model with nitrate isotope observations, Atmospheric Chemistry and Physics,  
520 20, 3859-3877, 10.5194/acp-20-3859-2020, 2020.

521 Atkinson, R.: Kinetics and mechanisms of the gas-phase reactions of the NO<sub>3</sub> radical  
522 with organic-comounds, Journal of Physical and Chemical Reference Data, 20,  
523 459-507, 10.1063/1.555887, 1991.

524 Baergen, A. M. and Donaldson, D. J.: Photochemical Renoxification of Nitric Acid on  
525 Real Urban Grime, Environmental Science & Technology, 47, 815-820,  
526 10.1021/es3037862, 2013.

527 Bao, F., Li, M., Zhang, Y., Chen, C., and Zhao, J.: Photochemical Aging of Beijing  
528 Urban PM<sub>2.5</sub>: HONO Production, Environmental Science & Technology, 52,  
529 6309-6316, 10.1021/acs.est.8b00538, 2018.

530 Bao, F., Jiang, H., Zhang, Y., Li, M., Ye, C., Wang, W., Ge, M., Chen, C., and Zhao, J.:  
531 The Key Role of Sulfate in the Photochemical Renoxification on Real PM<sub>2.5</sub>,  
532 Environmental Science & Technology, 54, 3121-3128, 10.1021/acs.est.9b06764,  
533 2020.

534 Bedjanian, Y. and El Zein, A.: Interaction of NO<sub>2</sub> with TiO<sub>2</sub> Surface Under UV  
535 Irradiation: Products Study, Journal of Physical Chemistry A, 116, 1758-1764,  
536 10.1021/jp210078b, 2012.

537 Brown, S. S., Osthoff, H. D., Stark, H., Dube, W. P., Ryerson, T. B., Warneke, C., de  
538 Gouw, J. A., Wollny, A. G., Parrish, D. D., Fehsenfeld, F. C., and Ravishankara, A. R.:

539 Aircraft observations of daytime  $\text{NO}_3$  and  $\text{N}_2\text{O}_5$  and their implications for  
540 tropospheric chemistry, *Journal of Photochemistry and Photobiology a-Chemistry*,  
541 176, 270-278, 10.1016/j.jphotochem.2005.10.004, 2005.

542 Burkholder, J. B., Talukdar, R. K., Ravishankara, A. R., and Solomon, S.:  
543 Temperature-dependence of the  $\text{HNO}_3$  UV absorption cross-sections, *Journal of*  
544 *Geophysical Research-Atmospheres*, 98, 22937-22948, 10.1029/93jd02178, 1993.

545 Chen, H., Nanayakkara, C. E., and Grassian, V. H.: Titanium Dioxide Photocatalysis  
546 in Atmospheric Chemistry, *Chemical Reviews*, 112, 5919-5948, 10.1021/cr3002092,  
547 2012.

548 Deng, J. J., Wang, T. J., Liu, L., and Jiang, F.: Modeling heterogeneous chemical  
549 processes on aerosol surface, *Particuology*, 8, 308-318, 10.1016/j.partic.2009.12.003,  
550 2010.

551 Dentener, F. J. and Crutzen, P. J.: Reaction of  $\text{N}_2\text{O}_5$  on tropospheric aerosols-impact  
552 on the global distributions of  $\text{NO}_x$ ,  $\text{O}_3$ , and OH, *Journal of Geophysical*  
553 *Research-Atmospheres*, 98, 7149-7163, 10.1029/92jd02979, 1993.

554 Du, J. and Zhu, L.: Quantification of the absorption cross sections of surface-adsorbed  
555 nitric acid in the 335-365 nm region by Brewster angle cavity ring-down spectroscopy,  
556 *Chemical Physics Letters*, 511, 213-218, 10.1016/j.cplett.2011.06.062, 2011.

557 Finlayson-Pitts, B. J. and Pitts, J. J. N.: *Chemistry of the Upper and Lower*  
558 *Atmosphere: Theory, Experiments and Applications*, 10.1023/A:1024719803484,  
559 Academic Press 1999.

560 Garcia, S. L. M., Pandit, S., Navea, J. G., and Grassian, V. H.: Nitrous Acid (HONO)  
561 Formation from the Irradiation of Aqueous Nitrate Solutions in the Presence of  
562 Marine Chromophoric Dissolved Organic Matter: Comparison to Other Organic  
563 Photosensitizers, *Acs Earth and Space Chemistry*, 5, 3056-3064,  
564 10.1021/acsearthspacechem.1c00292, 2021.

565 George, C., Ammann, M., D'Anna, B., Donaldson, D. J., and Nizkorodov, S. A.:  
566 Heterogeneous Photochemistry in the Atmosphere, *Chemical Reviews*, 115,  
567 4218-4258, 10.1021/cr500648z, 2015.

568 Goodman, A. L., Bernard, E. T., and Grassian, V. H.: Spectroscopic study of nitric

569 acid and water adsorption on oxide particles: Enhanced nitric acid uptake kinetics in  
570 the presence of adsorbed water, *Journal of Physical Chemistry A*, 105, 6443-6457,  
571 10.1021/jp003722l, 2001.

572 Harris, G. W., Carter, W. P. L., Winer, A. M., Pitts, J. N., Platt, U., and Perner, D.:  
573 Observations of nitrous-acid in the los-angeles atmosphere and implications for  
574 predictions of ozone precursor relationships, *Environmental Science & Technology*,  
575 16, 414-419, 10.1021/es00101a009, 1982.

576 Hot, J., Martinez, T., Wayser, B., Ringot, E., and Bertron, A.: Photocatalytic  
577 degradation of NO/NO<sub>2</sub> gas injected into a 10 m<sup>3</sup> experimental chamber,  
578 *Environmental Science and Pollution Research*, 24, 12562-12570,  
579 10.1007/s11356-016-7701-2, 2017.

580 Huang, L., Zhao, Y., Li, H., and Chen, Z.: Kinetics of Heterogeneous Reaction of  
581 Sulfur Dioxide on Authentic Mineral Dust: Effects of Relative Humidity and  
582 Hydrogen Peroxide, *Environmental Science & Technology*, 49, 10797-10805,  
583 10.1021/acs.est.5b03930, 2015.

584 Jiyeon, Park, Myoseon, Jang, Zechen, and Yu: Heterogeneous Photo-oxidation of SO<sub>2</sub>  
585 in the Presence of Two Different Mineral Dust Particles: Gobi and Arizona Dust,  
586 *Environmental Science & Technology*, 51, 9605-9613, 10.1021/acs.est.7b00588,  
587 2017.

588 Kasibhatla, P., Sherwen, T., Evans, M. J., Carpenter, L. J., Reed, C., Alexander, B.,  
589 Chen, Q., Sulprizio, M. P., Lee, J. D., Read, K. A., Bloss, W., Crilley, L. R., Keene, W.  
590 C., Pszenny, A. A. P., and Hodzic, A.: Global impact of nitrate photolysis in sea-salt  
591 aerosol on NO<sub>x</sub>, OH, and O<sub>3</sub> in the marine boundary layer, *Atmospheric Chemistry  
592 and Physics*, 18, 11185-11203, 10.5194/acp-18-11185-2018, 2018.

593 Kim, W.-H., Song, J.-M., Ko, H.-J., Kim, J. S., Lee, J. H., and Kang, C.-H.:  
594 Comparison of Chemical Compositions of Size-segregated Atmospheric Aerosols  
595 between Asian Dust and Non-Asian Dust Periods at Background Area of Korea,  
596 *Bulletin of the Korean Chemical Society*, 33, 3651-3656,  
597 10.5012/bkcs.2012.33.11.3651, 2012.

598 Lee, J. D., Moller, S. J., Read, K. A., Lewis, A. C., Mendes, L., and Carpenter, L. J.:

599 Year-round measurements of nitrogen oxides and ozone in the tropical North Atlantic  
600 marine boundary layer, *Journal of Geophysical Research-Atmospheres*, 114, D21302,  
601 10.1029/2009jd011878, 2009.

602 Lesko, D. M. B., Coddens, E. M., Swomley, H. D., Welch, R. M., Borgatta, J., and  
603 Navea, J. G.: Photochemistry of nitrate chemisorbed on various metal oxide surfaces,  
604 *Physical Chemistry Chemical Physics*, 17, 20775-20785, 10.1039/c5cp02903a, 2015.

605 Li, L., Wang, Q., Zhang, X., She, Y., Zhou, J., Chen, Y., Wang, P., Liu, S., Zhang, T.,  
606 Dai, W., Han, Y., and Cao, J.: Characteristics of single atmospheric particles in a  
607 heavily polluted urban area of China: size distributions and mixing states,  
608 *Environmental Science and Pollution Research*, 26, 11730-11742,  
609 10.1007/s11356-019-04579-3, 2019.

610 Li, X., Rohrer, F., Brauers, T., Hofzumahaus, A., Lu, K., Shao, M., Zhang, Y. H., and  
611 Wahner, A.: Modeling of HCHO and CHOCHO at a semi-rural site in southern China  
612 during the PRIDE-PRD2006 campaign, *Atmospheric Chemistry and Physics*, 14,  
613 12291-12305, 10.5194/acp-14-12291-2014, 2014.

614 Linsebigler, A. L., Lu, G. Q., and Yates, J. T.: Photocatalysis on TiO<sub>2</sub>  
615 surfaces-principles, mechanisms, and selected results, *Chemical Reviews*, 95,  
616 735-758, 10.1021/cr00035a013, 1995.

617 Ma, Q., Zhong, C., Ma, J., Ye, C., Zhao, Y., Liu, Y., Zhang, P., Chen, T., Liu, C., Chu,  
618 B., and He, H.: Comprehensive Study about the Photolysis of Nitrates on Mineral  
619 Oxides, *Environmental Science & Technology*, 55, 8604-8612,  
620 10.1021/acs.est.1c02182, 2021.

621 Maeda, N., Urakawa, A., Sharma, R., and Baiker, A.: Influence of Ba precursor on  
622 structural and catalytic properties of Pt-Ba/alumina NO<sub>x</sub> storage-reduction catalyst,  
623 *Applied Catalysis B-Environmental*, 103, 154-162, 10.1016/j.apcatb.2011.01.022,  
624 2011.

625 Monge, M. E., D'Anna, B., and George, C.: Nitrogen dioxide removal and nitrous  
626 acid formation on titanium oxide surfaces--an air quality remediation process?,  
627 *Physical Chemistry Chemical Physics*, 12, 8991-8998, 10.1039/b925785c, 2010.

628 Ndour, M., Conchon, P., D'Anna, B., Ka, O., and George, C.: Photochemistry of

629 mineral dust surface as a potential atmospheric renoxification process, *Geophysical*  
630 *Research Letters*, 36, 4, 10.1029/2008gl036662, 2009.

631 Ninneman, M., Lu, S., Zhou, X. L., and Schwab, J.: On the Importance of  
632 Surface-Enhanced Renoxification as an Oxides of Nitrogen Source in Rural and  
633 Urban New York State, *Acs Earth and Space Chemistry*, 4, 1985-1992,  
634 10.1021/acsearthspacechem.0c00185, 2020.

635 Ostaszewski, C. J., Stuart, N. M., Lesko, D. M. B., Kim, D., Lueckheide, M. J., and  
636 Navea, J. G.: Effects of Coadsorbed Water on the Heterogeneous Photochemistry of  
637 Nitrates Adsorbed on TiO<sub>2</sub>, *Journal of Physical Chemistry A*, 122, 6360-6371,  
638 10.1021/acs.jpca.8b04979, 2018.

639 Pandit, S., Garcia, S. L. M., and Grassian, V. H.: HONO Production from Gypsum  
640 Surfaces Following Exposure to NO<sub>2</sub> and HNO<sub>3</sub>: Roles of Relative Humidity and  
641 Light Source, *Environmental Science & Technology*, 55, 9761-9772,  
642 10.1021/acs.est.1c01359, 2021.

643 Platt, U., Perner, D., Harris, G. W., Winer, A. M., and Pitts, J. N.: Observations of  
644 nitrous-acid in an urban atmosphere by differential optical-absorption, *Nature*, 285,  
645 312-314, 10.1038/285312a0, 1980.

646 Read, K. A., Mahajan, A. S., Carpenter, L. J., Evans, M. J., Faria, B. V. E., Heard, D.  
647 E., Hopkins, J. R., Lee, J. D., Moller, S. J., Lewis, A. C., Mendes, L., McQuaid, J. B.,  
648 Oetjen, H., Saiz-Lopez, A., Pilling, M. J., and Plane, J. M. C.: Extensive  
649 halogen-mediated ozone destruction over the tropical Atlantic Ocean, *Nature*, 453,  
650 1232-1235, 10.1038/nature07035, 2008.

651 Reed, C., Evans, M. J., Crilley, L. R., Bloss, W. J., Sherwen, T., Read, K. A., Lee, J.  
652 D., and Carpenter, L. J.: Evidence for renoxification in the tropical marine boundary  
653 layer, *Atmospheric Chemistry and Physics*, 17, 4081-4092,  
654 10.5194/acp-17-4081-2017, 2017.

655 Romer, P. S., Wooldridge, P. J., Crouse, J. D., Kim, M. J., Wennberg, P. O., Dibb, J.  
656 E., Scheuer, E., Blake, D. R., Meinardi, S., Brosius, A. L., Thames, A. B., Miller, D.  
657 O., Brune, W. H., Hall, S. R., Ryerson, T. B., and Cohen, R. C.: Constraints on  
658 Aerosol Nitrate Photolysis as a Potential Source of HONO and NO<sub>x</sub>, *Environmental*

659 Science & Technology, 52, 13738-13746, 10.1021/acs.est.8b03861, 2018.

660 Rosseler, O., Sleiman, M., Nahuel Montesinos, V., Shavorskiy, A., Keller, V., Keller,  
661 N., Litter, M. I., Bluhm, H., Salmeron, M., and Destailats, H.: Chemistry of NO<sub>x</sub> on  
662 TiO<sub>2</sub> Surfaces Studied by Ambient Pressure XPS: Products, Effect of UV Irradiation,  
663 Water, and Coadsorbed K<sup>+</sup>, Journal of Physical Chemistry Letters, 4, 536-541,  
664 10.1021/jz302119g, 2013.

665 Schuttlefield, J., Rubasinghege, G., El-Maazawi, M., Bone, J., and Grassian, V. H.:  
666 Photochemistry of adsorbed nitrate, Journal of the American Chemical Society, 130,  
667 12210-12211, 10.1021/ja802342m, 2008.

668 Schutze, M. and Herrmann, H.: Uptake of the NO<sub>3</sub> radical on aqueous surfaces,  
669 Journal of Atmospheric Chemistry, 52, 1-18, 10.1007/s10874-005-6153-8, 2005.

670 Schwartz-Narbonne, H., Jones, S. H., and Donaldson, D. J.: Indoor Lighting Releases  
671 Gas Phase Nitrogen Oxides from Indoor Painted Surfaces, Environmental Science &  
672 Technology Letters, 6, 92-97, 10.1021/acs.estlett.8b00685, 2019.

673 Seltzer, K. M., Vizuete, W., and Henderson, B. H.: Evaluation of updated nitric acid  
674 chemistry on ozone precursors and radiative effects, Atmospheric Chemistry and  
675 Physics, 15, 5973-5986, 10.5194/acp-15-5973-2015, 2015.

676 Shang, J., Xu, W. W., Ye, C. X., George, C., and Zhu, T.: Synergistic effect of  
677 nitrate-doped TiO<sub>2</sub> aerosols on the fast photochemical oxidation of formaldehyde,  
678 Scientific Reports, 7, 1161, 10.1038/s41598-017-01396-x, 2017.

679 Shi, Q., Tao, Y., Krechmer, J. E., Heald, C. L., Murphy, J. G., Kroll, J. H., and Ye, Q.:  
680 Laboratory Investigation of Renoxification from the Photolysis of Inorganic  
681 Particulate Nitrate, Environmental science & technology, 55, 854-861,  
682 10.1021/acs.est.0c06049, 2021.

683 Stemmler, K., Ammann, M., Donders, C., Kleffmann, J., and George, C.:  
684 Photosensitized reduction of nitrogen dioxide on humic acid as a source of nitrous  
685 acid, Nature, 440, 195-198, 10.1038/nature04603, 2006.

686 Sun, Y. L., Zhuang, G. S., Wang, Y., Zhao, X. J., Li, J., Wang, Z. F., and An, Z. S.:  
687 Chemical composition of dust storms in Beijing and implications for the mixing of  
688 mineral aerosol with pollution aerosol on the pathway, Journal of Geophysical

689 Research-Atmospheres, 110, D24209, 10.1029/2005jd006054, 2005.

690 Tang, M., Liu, Y., He, J., Wang, Z., Wu, Z., and Ji, D.: In situ continuous hourly  
691 observations of wintertime nitrate, sulfate and ammonium in a megacity in the North  
692 China plain from 2014 to 2019: Temporal variation, chemical formation and regional  
693 transport, *Chemosphere*, 262, 10.1016/j.chemosphere.2020.127745, 2021.

694 Tian, S. S., Liu, Y. Y., Wang, J., Wang, J., Hou, L. J., Lv, B., Wang, X. H., Zhao, X. Y.,  
695 Yang, W., Geng, C. M., Han, B., and Bai, Z. P.: Chemical Compositions and Source  
696 Analysis of PM<sub>2.5</sub> during Autumn and Winter in a Heavily Polluted City in China,  
697 *Atmosphere*, 11, 19, 10.3390/atmos11040336, 2020.

698 Verbruggen, S. W.: TiO<sub>2</sub> photocatalysis for the degradation of pollutants in gas phase:  
699 From morphological design to plasmonic enhancement, *Journal of Photochemistry  
700 and Photobiology C-Photochemistry Reviews*, 24, 64-82,  
701 10.1016/j.jphotochemrev.2015.07.001, 2015.

702 Wang, H., Miao, Q., Shen, L., Yang, Q., Wu, Y., Wei, H., Yin, Y., Zhao, T., Zhu, B.,  
703 and Lu, W.: Characterization of the aerosol chemical composition during the  
704 COVID-19 lockdown period in Suzhou in the Yangtze River Delta, China, *Journal of  
705 environmental sciences (China)*, 102, 110-122, 10.1016/j.jes.2020.09.019, 2021.

706 Wang, Z., Ma, Y., Zheng, J., Li, S., Wang, L., and Zhang, Y.: Source apportionment of  
707 aerosols in urban Nanjing based on particle size distribution, *Huanjing  
708 Huaxue-Environmental Chemistry*, 34, 1619-1626,  
709 10.7524/j.issn.0254-6108.2015.09.2015020303, 2015.

710 Wayne, R. P., Barnes, I., Biggs, P., Burrows, J. P., Canosamas, C. E., Hjorth, J., Lebras,  
711 G., Moortgat, G. K., Perner, D., Poulet, G., Restelli, G., and Sidebottom, H.: The  
712 nitrate radical-physics, chemistry, and the atmosphere, *Atmospheric Environment Part  
713 a-General Topics*, 25, 1-203, 10.1016/0960-1686(91)90192-a, 1991.

714 Ye, C., Gao, H., Zhang, N., and Zhou, X.: Photolysis of Nitric Acid and Nitrate on  
715 Natural and Artificial Surfaces, *Environmental Science & Technology*, 50, 3530-3536,  
716 10.1021/acs.est.5b05032, 2016a.

717 Ye, C., Zhang, N., Gao, H., and Zhou, X.: Photolysis of Particulate Nitrate as a Source  
718 of HONO and NO<sub>x</sub>, *Environmental Science & Technology*, 51, 6849-6856,



719 10.1021/acs.est.7b00387, 2017.

720 Ye, C., Zhou, X., Pu, D., Stutz, J., Festa, J., Spolaor, M., Tsai, C., Cantrell, C.,  
721 Mauldin, R. L., III, Campos, T., Weinheimer, A., Hornbrook, R. S., Apel, E. C.,  
722 Guenther, A., Kaser, L., Yuan, B., Karl, T., Haggerty, J., Hall, S., Ullmann, K., Smith,  
723 J. N., Ortega, J., and Knote, C.: Rapid cycling of reactive nitrogen in the marine  
724 boundary layer, *Nature*, 532, 489-491, 10.1038/nature17195, 2016b.

725 Zhou, J. B., Xing, Z. Y., Deng, J. J., and Du, K.: Characterizing and sourcing ambient  
726 PM<sub>2.5</sub> over key emission regions in China I: Water-soluble ions and carbonaceous  
727 fractions, *Atmospheric Environment*, 135, 20-30, 10.1016/j.atmosenv.2016.03.054,  
728 2016.

729 Zhou, X. L., Gao, H. L., He, Y., Huang, G., Bertman, S. B., Civerolo, K., and Schwab,  
730 J.: Nitric acid photolysis on surfaces in low-NO<sub>x</sub> environments: Significant  
731 atmospheric implications, *Geophysical Research Letters*, 30, 2217,  
732 10.1029/2003gl018620, 2003.

733